Transitions to spike-wave oscillations and epileptic dynamics in a human cortico-thalamic mean-field model.

Serafim Rodrigues, David Barton, Robert Szalai, Oscar Benjamin, Mark P. Richardson[(*)] and John R. Ter

Department of Engineering Mathematics, University of Bristol, BS8 1TR, United Kingdom.

[(*)]Institute of Psychiatry, King's College London, Camberwell, SE5 8AF

April 22, 2008

Abstract

In this paper we present a detailed theoretical analysis of the onset of spike-wave activity in a model of human EEG activity, relating this to clinical recordings from patients with absence seizures. We present a complete explanation of the transition from healthy activity to spike and wave using a combination of bifurcation theory, numerical continuation and techniques for detecting the occurrence of inflection points in systems of DDEs. We observe the the initial transition to oscillatory behaviour occurs as a result of a Hopf bifurcation, whereas the addition of spikes arises as a result of an inflection point of the vector field. Strikingly these findings are consistent with EEG data recorded from patients with absence seizures and we present a discussion of the clinical significance of these results, suggesting potential new techniques for detection and anticipation of seizures.

PACS: 87.10.+e, 87.19.-j, 87.18.-h 05.45.-a

Keywords: Mathematical EEG modelling, cortico-thalamic model, spike-wave oscillations.

1 Introduction

Absence seizures, a class of primary generalised seizures, are associated with pathological brain rhythms involving bilateral thalamo-cortical circuits and are associated with loss of awareness and behavioural arrest. During EEG monitoring, a classic pattern of three per second, bilaterally synchrononous spike and wave (SW) discharges can be observed. These oscillations slow only slightly during the seizure but does not alter significantly in morphology. Seizure activity typically lasts for only a few seconds, with an abrupt onset and offset. Subjects have no memory of the event post-ictally. Since seizures can occur tens or hundreds of times a day, this disorder can have a profound impact on educational and work performance, as well as social behaviour.

The cause of this pathology is presumably genetic, however genetic abnormalities responsible for absence phenotype in humans are not yet clear in the vast majority of cases [Crunelli and Lersche (2002)]. Animal models of absence seizures, such as the Wistar albino Glaxo from Rijswijk (WAG/Rij) [Coenen and Luijtelaar (1986), van Luijtelaar *et al. (2003)*] rat or the generalised absence epilepsy rat from Strasbourg (GAERS) [Marescaux *et al. (* Donober *et al. (1998)*] have implicated abnormalities in the cortical and thalamic activity in the generation of absence seizures [Steriade and Contreras (1998), Steriade *et al. (1998)*]. Computational models of thalamocortical circuits involved in SW generation have advanced our understanding of some neuronal mechanisms underlying this pathology [Wang *et al. (1995)*, Destexhe and Sejnowski (2001)]. However, understanding of the underlying physiological processes is still fragmentary, resulting in limited understanding of the role played by different mechanisms in the process of seizure generation.

The overwhelming complexity of neuronal processes involved and how these evolve spatio-temporally favours a different modelling approach. During an absence seizure, the brain enters a hypersynchronous

state entraining population of neurons to the same dynamic activity. Equally, EEG pontentials that are readily available and often used to clinically diagnose the pathology result from aggregate activity of large masses of neurons. Consequently, since 1970s it has been increasingly realised that an effective way to model these populations is to adopt a mean-field approach, in which individual spike times are ignored in favour of tracking firing rate and lumping parameters, averaged over sub-mm scales [Wilson and Cowan (1972), Lopes da Silva *et al. (1974)*, Freeman (1975)]. The correspondence between distributed neuronal networks and population models was established theoretically in [Wilson and Cowan (1972)] and later experimentally by [Freeman (1975)], which provided a formal methodology to compare macroscopic quantities, such as EEG recordings, to continuous variables. The advantage of this approach is that it allows to investigate dynamical properties of a neuronal system and the role played by different physiological mechanisms, both at short and long time scales.

Mean-field models have yielded a range of experimentally verified predictions for phenomena including steady firing rates, basic properties of waves of cortical electrical activity, EEG spectra, evoked response potentials, correlation and coherence properties of EEGs, and spatial structure [Wilson and Cowan (1972), Lopes da Silva *et al. (1974)*, Freeman (1975), Nunez (1981), Jirsa and Haken (1996), Wright and Liley (1996), Robinson *et al. (1997)*]. In particular, our previous study demonstrates the predictive and descriptive validity of this approach in modelling a wide range of healthy states and specific properties of generalised seizures in humans [Breakspear *et al. (2005)*]. The aim of the study was to contrast clinical research suggesting that several pathological processes, such as seizures and abnormal rhythms have a strong nonlinear component [Stam *et al. (1997)*, Stam and Pritchard (1999), Andrezejak *et al. (2001)*], as opposed to healthy states having predominantly a linear/stochastic phenomena with intermittent weakly nonlinear fluctuations in the alpha band (8-13Hz) [Stam *et al. (1999)*, Breakspear and Terry (2002b), Breakspear and Terry (2002a)]. In addition, from a modelling perspective, the concept of epilepsy as a

dynamic disease has become widely recognised [Lopes da Silva and Pijn (1999), Lopes da Silva *et al. (2003)*]. In this case, the disease is characterised by sudden qualitative changes in system behaviour without alteration to external conditions.

Further studies in this area [Robinson *et al. (2001)*, Robinson *et al. (2002)*], produced evidence that cortico-thalamic mean-field models could produce a variety of resting and sleeping human EEG properties when evolving in a stable, weakly damped linear regime. This view of only occasional and weak nonlinearity also finds strong support in the success of classic functional neuroscience algorithms which are rooted in a stochastic/linear framework [Friston *et al. (1994)*]. In addition, this study provided novel insight, arguing that the transition from resting-state to seizure activity results from an instability that yields nonlinear oscillations in the brain's electric activity, whereas different types of seizures may be viewed as bifurcations between distinct types of nonlinear dynamics, see also [Wendling *et al. (2002)*, Lopes da Silva *et al. (2003)*]. Other mean-field models found similar conclusions when modelling rat absence seizures, which slightly differ from human absence seizure [Suffczynski (2000), Suggczynski *et al. (2004)*].

Developing this mean-field approach, predictions of the stability boundaries using the cortico-thalamic model proposed by Robinson were further studied and outlined in our previous work [Breakspear *et al. (2005)*]. Here the onset of seizures occurred due to a transition from a stable linear dynamics to limit cycles oscillations via a Hopf bifurcation. Further, in the case of absence seizures, it was shown that as a physiological parameter was uniformly increased the limit cycle evolved dynamically from sinusoidal-like activity to SW oscillations. However, the exact mechanism giving rise to the onset of SW morphology remained unclear and the overall dynamics of absence seizures were captured through numerical simulations only. Subsequently, we presented an explanation for the onset of SW phenomena in [Rodrigues *et al. (2006)*].

Although insightful, this explanation was limited due to the model reductions and assumptions made.

In this present work, we fully investigate the transitions to SW and its genesis, suggesting mechanisms that could be investigated using novel experimental paradigms, provide new directions for model enhancement and crucially inform clinical neuroscience. The findings we present provide an explanation of human EEG seizure data that provides insight to seizure initiation, propagation and termination, thus providing an alternative approach in these areas from more traditional signal processing perspectives [Mormann *et al. (2005)*].

2 Description of the model

The model described and analysed herein stems from [Robinson *et al. (2002)*]. This system may be thought of as a merger of three contrasting theoretical viewpoints. First, Freeman's mass action to describe the population dynamics within a macrocolumn [Freeman (1975)]. Second, the thalamocortical feedback loop as a physiologically motivated feature to allow interpretation of generalised seizures at the macroscopic level. Finally, the formalism to model EEG wave propagation on the cortical surface, using a wave-like equation [Jirsa and Haken (1996)]. Given that the model is formulated within these three theoretical standpoints, it inherits the assumptions made by each. Because of this, it should be denoted a neural-mass cortico-thalamic model, which for brevity we typically refer to as a cortico-thalamic model. The model also includes a further refinement to account for signal propagation delays in the thalamo-cortical and cortico-thalamic projections.

The thalamo-cortical loop hypothesises that four main types of neurons are involved in generalised seizures. These are excitatory and inhibitory neuron populations in both cortex and thalamus [Steriade and Contreras Steriade *et al. (1998)*, Destexhe and Sejnowski (2001)]. The hyper-synchronised state of local neurons

observed in generalised seizures makes it reasonable to group and average over each population. The dynamical variables within a population of type a are the local mean membrane potential, V_a; the mean firing rate, ς_a and the axonal field, ϕ_a. Consequently, each population is governed by the following three equations:

$$\left[\frac{1}{\alpha\beta}\frac{\partial^2}{\partial t^2} + (\frac{1}{\alpha} + \frac{1}{\beta})\frac{\partial}{\partial t} + 1\right] V_a(r,t) = P_a(r,t), \tag{1}$$

$$\varsigma_a(r,t) = \frac{Q_a^{max}}{1 + \exp\left(-\frac{\pi}{\sqrt{3}}(\frac{V_a(r,t)-\theta_a}{\sigma_a})\right)}, \tag{2}$$

$$\left[\frac{\partial^2}{\partial t^2} + 2\gamma_a\frac{\partial}{\partial t} + \gamma_a^2 - \nu_a^2\nabla^2\right]\phi_a(r,t) = (\gamma_a^2 - \gamma_a\frac{\partial}{\partial t})\varsigma_a(r,t). \tag{3}$$

The specific neuron populations we consider are denoted e (*excitatory pyramidal cells*), i (*inhibitory inter-neurons*), s (*specific relay nuclei*) and r (*reticular nucleus*). Further, n represents nonspecific subthalamic inputs and r is the spatial location of the measured activity. Equation (1) corresponds to the activation of the voltage, $V_a(r,t)$, of a neuronal population a in response to incoming averaged postsynaptic potentials $P_a(r,t)$ after these have been filtered in the dendritic tree and summed. Equation (2) refers to the mean firing rate $\varsigma_a(r,t)$ (sometimes called the pulse density), with average threshold denoted by θ_a. In other words, $V_a(r,t)$, determines the output firing rate of the neuronal population and the level of activity is modulated by a response probability sigmoidal function $\varsigma[V_a(r,t)]$. This response function is a smooth transition from 0 to Q_a^{max} (maximum firing rate), with standard deviation, σ_a, that reflects the variation of threshold levels encountered in real populations. Note that the maximum of $\frac{dQ_a}{dV_a}$ is $\frac{CQ_a^{max}}{4\sigma_a}$ at $V_a = \theta_a$ and the constant $C = \frac{1}{\sqrt{3}}$ was chosen so that the $\frac{dQ_a}{dV_a}$ approximates a Gaussian. The last equation (3) is the wave-like equation developed by Jirsa and Haken [Jirsa and Haken (1996)] to model the propagation of the firing rates ς_a as fields ϕ_a. The RHS of equation (3) is neglected as it does not appear to influence numerical simulations [Robinson *et al. (2002)*]. A characteristic axonal propagation velocity, $v_a = 6 - 10\ ms^{-1}$, is assumed as well as an isotropic distribution of axons.

Linking the above equations for each cortical and thalamic population gives rise to a high dimensional

system of equations, and so reductions of this system are sought. Reducing a system of equations should be carefully considered and any reduction should lie within the limits of physiological constraints. Care must be taken as there are significant differences in the mechanisms underlying the spread of activity in cortical and thalamic slices. Computational models and experimental animal studies of spindle waves and epilepsy, indicate that thalamic slices waves propagate at velocities of less than $1\ cm/s$ whereas cortical discharges propagate with velocities in the range $6-10\ ms^{-1}$ [Destexhe and Sejnowski (2001)]. These differences in velocities are attributable to axonal ranges within each brain area: within the thalamus as a whole and an individual cortical column, axons of both excitatory and inhibitory neurons project closely to nearby neurons. This observation allows a reduction of the wave-like equation to $\phi_a = \varsigma_a(r,t)$, where $\gamma_a \to \infty$. However, between cortical columns, only pyramidal cells project their axons to other cortical regions (long range connections) and these fields are what are believed to be measured using EEG. Hence, equation (3) is only applied to the excitatory pyramidal neuron population of the cortex. It is worth noting that this wave equation indirectly introduces delays within these connections. For cortico-thalamic connectivity, connections are assumed to be long-range due to the distance between cortex and thalamus. Since the activity of the cortico-thalamic and thalamo-cortical projections are not readily measurable via EEG, the wave equation is dropped for these connections. However, the activation of one brain region by another depends on the rise times of post-synaptic potentials and delays due to the finite velocity of action potential propagation, which introduces delays in cortico-thalamic and thalamo-cortical interactions. A final assumption is that incoming fields from different neuronal populations are linearly summed via the dendrites of each. Thus, the coupling between the different neural populations is defined as follows:

$$D_\alpha V_e(r,t) = \nu_{ee}\phi_e(r,t) + \nu_{ei}\phi_i(r,t) + \nu_{es}\phi_s(r,t-\tau), \tag{4}$$

$$D_\alpha V_i(r,t) = \nu_{ie}\phi_e(r,t) + \nu_{ii}\phi_i(r,t) + \nu_{is}\phi_s(r,t-\tau), \tag{5}$$

$$D_\alpha V_r(r,t) = \nu_{re}\phi_e(r,t-\tau) + \nu_{rs}\phi_s(r,t), \tag{6}$$

$$D_\alpha V_s(r,t) = \nu_{se}\phi_e(r,t-\tau) + \nu_{sr}\phi_r(r,t) + \nu_{sn}\phi_n(r,t), \tag{7}$$

where $D_\alpha = \left[\frac{1}{\alpha\beta}\frac{\partial^2}{\partial t^2} + (\frac{1}{\alpha}+\frac{1}{\beta})\frac{\partial}{\partial t} + 1\right]$, $\tau = t_0/2$, with t_0 considered to be the total propagation time for signals to project to the cortex and return back to the thalamus. Only the specific relay nuclei (s) receive sensory inputs ϕ_n which may be either a time invariant signal or noise. In the present study we only consider the former case. The model is further reduced by dropping equation (5), for the cortical inhibitory population. This is because of an assumed existence of a spatial symmetry between populations of pyramidal cells and inhibitory interneurons [Robinson *et al. (2002)*]. The argument presented therein is that intracortical connectivities are proportional to the numbers of synapses involved, which implies $V_i = V_e$ and $Q_i = Q_e$. Finally, as we are considering generalized seizures, it is believed that dynamical processes involved occur simultaneously throughout the cortex. Thus we lose the spatial variable r and consequently the Laplacian term, $\nu_a^2\nabla^2$, along with the boundary conditions dependent on r are ignored. In this case only global invariant solutions can be considered. We may then rewrite equations (1) and (3) in first order form for all the neuronal populations which results the cortico-thalamic model given in Appendix-(§A.1) represented heuristically as follows:

$$\begin{cases} \dot{x} = F(x(t), x(t-\tau), \nu), \quad t > 0 \\ x(t) = \varphi(t), \quad t \leq 0 \end{cases} \tag{8}$$

where $F \in C^k(\mathbb{R}^{2*8} \times \mathbb{R}^{15}, \mathbb{R}^8)$ and $\tau \in \mathbb{R}$ is the fixed delay. $\nu \in \mathbb{R}^{15}$ is the total parameter space, but in this present study, the only parameter of interest is the cortico-thalamic synaptic strength, $\nu_{se} \subset \nu$, due to its physiological relevance in studies of absence seizures [Destexhe and Sejnowski (2001), Robinson *et al. (2002)*]. A complete description of all other parameters can be found in table (1) and a schematic of the model can be seen in the Fig. (2). The initial conditions $\varphi : [-\tau, 0] \to \mathbb{R}^8$ of the evolution equation are also given in the Appendix-(§A.2). The dynamics of the model evolve from these initial conditions to give spike-wave activity.

3 Delay differential equations and Computational methods

Mathematically, system (8) is a system of delay differential equations (DDEs). The state of the system at time $t > 0$ is a continuous function of the time interval [$t - \tau$, t], which is an evolution of the initial condition, $\varphi(t)$, defined on the time interval [-τ,0]. Therefore the phase space of the system is an infinite dimensional space of continuous functions with values in the state space $\mathbb{R}^8$. The purpose of our study is to explain the onset of spike-wave oscillations and describe the bifurcations that give rise to this state. To do this we make use of two continuation packages, DDE-BIFTOOL [Engelborghs *et al. (2001)*] and PDDE-CONT [Szalai *et al. (2006)*]. PDDE-CONT is a software package written in C++ for continuation of periodic solution bifurcations of autonomous and periodically forced delay-differential equations. It can continue periodic solutions one or two parameter space. The stability of solutions are determined by computing finitely many Floquet multipliers and bifurcation points are detected by test-functionals. The package detects period doubling, saddle-node bifurcations of limit cycles and Neimark-Sacker (torus) bifurcations. Moreover, a limited number of codimension-two bifurcations can be continued, when two different test-functionals are selected. Equilibria of autonomous systems can be continued as a constant periodic orbit with fixed period. In this case, Hopf bifurcations are detected as Neimark-Sacker bifurcations and the periodic solution, emanating from the Hopf point, can be continued by switching to the periodic solution branch. Since continuing equilibria in this way is very inefficient, one can avoide this by computing starting points using DDE-BIFTOOL or from simulation.

DDE-BIFTOOL consists of Matlab routines for the bifurcation analysis of steady states and periodic solutions for autonomous delay equations only. This package differs from PDDE-CONT in that different algorithms are employed to continue solution branches. In particular, steady states are not continued as periodic orbits with fixed period. DDE-BIFTOOL detects local bifurcations, including saddle node bifurcations, Hopf bifurcations, period-doubling bifurcations, and saddle-node bifurcations of limit cycles.

Furthermore, extra conditions during corrections and continuation of solution branches can be added. This enables user boundary value problems to be defined, which allows tracking of a familiy of periodic orbits specified by these conditions.

In our previous work [Breakspear *et al. (2005)*], we simulated the system (8) using a *fourth order Runge-Kutta* and *cubic spline interpolation* methods [Arndt (1989), Paul (1992)]. However, because we the system (8) is stiff and has a single fixed delay, it is preferable to consider a method that uses the time delay as an integer multiple of the time step. In the present study, we instead use the *Adams-Bashforth fourth order multistep* scheme [Hairer and Wanner (1996), Hairer *et al. (1993)*, Baker *et al. (1995)*, Kim and Pimenov (1997), Paul (1992)], which avoids the need for interpolation. In order to integrate this DDE (8), we discretise the state state, x, on the time interval $[t-\tau,\ t]$ using N subintervals. This leads to an integration time-step of τ/N. In particular, the *Adams-Bashforth* method requires knowledge of values up to and including $x(-\tau-3(\tau/N))$ for each integration step. This scheme improves bifurcation diagrams obtained numerically, particularly when dynamical attractors exist for only a tiny window of parameter space. Specifically, we find that for system (8), chaotic dynamics do exist, but only for very tiny regions of parameter space that the *fourth order Runge-Kutta* method fails to capture. However, it should be noted that the alteration in the numerical method does not alter the predictions and conclusions made in [Breakspear *et al. (2005)*].

4 Model prediction of absence seizure

Our recent work carried out in [Breakspear *et al. (2005)*] showed that by employing a combination of nonlinear analysis tools and numerical bifurcation theory, the cortico-thalamic model (11) can explain the transition from healthy waking states to generalised seizure states. In particular, we demonstrated that transitions to pathological oscillations occurred upon varying specific parameters. In the case of

absence seizures, this was as a result of increasing a single parameter, ν_{se}, governing the strength of synaptic interactions between cortex and specific relay nuclei. Most importantly, good agreement between dynamics of the model and transitions observed in clinical EEG data was demonstrated. In this study we provide a complete understanding of the governing dynamics of the transition to absence seizures in the model, by describing the mechanisms for the appearance of spike-wave oscillations.

A plot of a noise free bifurcation diagram showing the transition from healthy states (steady state) to pathologic oscillations is presented in Fig (2). This is obtained by numerically simulating the system and plot (after vanishing transients) the maximum and minimum amplitude of the cortical activity, ϕ_e, as the parameter of interest, ν_{se}, is uniformly increased. This technique is useful to numerically consider bifurcations of stable attractors. In particular, approximate $3Hz$ oscillatory activity occurs as a result of a Hopf bifurcation for $\nu_{se} \approx 0.002$, using initial conditions given in Appendix-(§A.2). The parameter is then varied to study the geometry of the bifurcation set. Beyond the Hopf bifurcation, extra structure appears between $\nu_{se} \approx 3.9 \times 10^{-3} Vs$ and $\nu_{se} \approx 6.05 \times 10^{-3} Vs$, which for the sake of discussion we denote the 'spike bifurcation', as spike-wave oscillations are observed in the simulated time-series data beyond this point. Further increasing ν_{se} gives rise to a small window of period doubling bifurcations that comence at $\nu_{se} \approx 6.055 \times 10^{-3} Vs$ and lead to chaotic dynamics. The inset of Fig (2) shows in detail the chaotic dynamics and the bottom panels are examples of time series generated in this parameter window. The bottom left panel illustrate oscillations at parameter $\nu_{se} \approx 6.1 \times 10^{-3} Vs$, whereas the right panel depicts a time profile of chaotic oscillations. A further variation in, ν_{se}, causes the termination of the oscillations, resulting in a steady-state corresponding to the maximum assumed firing rate of the neuronal population. We reiterate the point made in the previous section about the *fourth order Runge-Kutta* scheme previously used being unable to capture this transition to chaotic dynamics, instead a transition from periodic spike-wave activity to maximum firing is observed. We direct the reader to compare Fig (2) and Fig (3-a) or Fig (11-e) of our previous work in [Breakspear *et al. (2005)*].

Note that Fig (11) of the same work, represents a homotopy of parameter sets corresponding to absence seizures and generalized tonic-clonic seizures. A linear variation of the parameters from one state to the other results in chaotic dynamics being observed over a wider region of parameter space, see Fig (11-d). In this case the *fourth order Runge-Kutta* scheme accurately captures the overall dynamics.

A comparison between clinical EEG data recorded during an absence seizure and the numerical bifurcation diagram is depicted in Fig (3), which shows the onset of seizure and $3Hz$ paroxysmal oscillations. The result demonstrates our current working hypothesis which suggests that the underlying dynamics of EEG recordings during absence seizures is governed by a Hopf bifurcation as predicted from the model upon varying ν_{se}. A further increase in ν_{se} elicits the 'spike-bifurcation', which are the hallmark of absence seizures. In our previous study [Breakspear *et al. (2005)*], the unfolding of the 'spike bifurcation' remained unclear as DDE-Biftool did not flag a change in structural stability in the model. Initially we believed a global bifurcation or the possibility of a torus bifurcation, where a new frequency is born, could explain the initiation of spike-wave oscillations. However, after careful inspection of time series generated from the model and by calculating Floquet multipliers these were ruled out. Instead we find that as the parameter ν_{se} is uniformly increased the oscillations deform *smoothly* from sinusoidal like waveforms to a new waveform with an additional spike per period, rather than as a result of an abrupt change in structural stability, as would be expected in a bifurcation. Moreover, this smooth deformation of the periodic solution arises as a consequence of a change in curvature of the oscillation, due to an inflection point. Thus, if the solution of the vector field (8) satisfies simultaneously at some instance in time, t_0, the conditions: $\dot{x}(t_0) = 0$ and $\dot{x}(t_0) = 0$, then the additional spike will occur. i.e. it is this change in curvature that gives rise to the spike-wave activity observed in the model dynamics. We will return to this discussion later to understand the effect of the delay on these paroxysmal oscillations.

To investigate the robustness of these findings and to understand the variability in spike-wave oscillations arising as a result of this small chaotic region, we use numerical continuation of solution branches via PDDE-CONT and DDE-BIFTOOL in tandem (see Figure (5)). As well as confirming the numerical results presented in Fig (2), we may also consider unstable solutions and bifurcations thereof. Numerical continuation provides further insight into the appearance and subsequent annihilation of pathological oscillations, as the parameter of interest ν_{se} is varied. It is important to note that the model as written exhibits multistability, with steady state solutions (corresponding to maximal firing of the population and to the alpha rhythm) coexisting for values of the parameter in the range $8.4 \times 10^{-4} Vs \leq \nu_{se} \leq 2 \times 10^{-3} Vs$. These two branches are connected via saddle nodes at LP1 and LP2. There is also a coexistence between the maximal firing and pathological oscillations for values of the parameter in the range $2 \times 10^{-3} Vs \leq \nu_{se} \leq 6.21 \times 10^{-3} Vs$. It is this second region that we focus on, as the unfolding of the spike-wave oscillation occurs here.

Starting at the lower steady state branch and smoothly increasing, ν_{se}, a Hopf bifurcation, HB1, is born from which emanates a pathalogical oscillation causing stability loss of the steady state corresponding to alpha activity. A continuation of the branch of periodic solutions that arises from HB1 shows a gradual increase in amplitude, reaching a maximum at $\phi_e = 40.64$, where a period doubling, PD1, is encountered. Along the branch HB1-PD1 the frequency of oscillations remains fairly constant around $T \approx 3.4 Hz$. Fig (6), further complements these results by considering an enlargement of this region. Continuing the branch from which the period doubling PD1 is born, we observe that the branch loses stability when it gains maximal amplitude $\phi_e = 43.27$ at a second period doubling, PD2. An example of a solution profile belonging to branch PD1-PD2 is given in the right hand panel of Fig (6). These doublings result in solutions that resemble more complex polyspike-wave activity that is observed in clinical recordings, for example a 'spike-wave-spike' before a single spike-wave in each period. It is also consistent with studies of absence seizures employing autoregressive nonlinear signal analysis techniques,

which show that combinations of time-delayed nonlinear (quadratic) terms can explain a variety of spike and wave morphologies [Schiff *et al. (1995)*]. Following the branch which emanates from the second period doubling, PD2, equally sees an increase in amplitude and quadrupling in period relative to HB1. This branch loses stability where yet another period doubling, PD5, is born. An illustration of a solution profile along this branch is depicted in Fig (6), observe the middle right panel that shows a transformation of the solution profile to two alternating 'spike-wave-spike' and spike-wave complexes.

Following the latter branches suggests a period doubling cascade, possibly leading to chaos. This result explains the chaotic behaviour obtained by numerical simulations shown in Fig (2). After PD5 the computations become progressively more difficult but, somewhat surprisingly, the branch of periodic solutions regains stability. This phenomena can be seen by the continuation diagrams Fig (5)-(6) illustrating that when PD1 is born the branch of pathological oscillations emanating from HB1 becomes unstable but regains stability at, PD6, where a saddle node of periodic orbits, SNP2, occurs. An example of the periodic orbits of this stable region is illustrated in Fig (6 - top right panel), which shows that these solutions have spike-wave-spike complexes with the second spike having a more prominent amplitude. Further continuing this branch through the period doubling, PD4, we find that the unstable branch turns back on it self a number of times until no further changes are observed in the continuation diagram.

These accumulating branches of unstable periodic orbits (observed in the inset of Fig (4)) is alternatively explained via Fig (7) and its corresponding enlargement, Fig (8). The branches were continued as far as computationally tractable and these show accumulating behaviour persisting throughout the parameter space (ν_{se}, T), as the period of oscillations, T, tends to infinity. The behaviour shown in Fig(s) (7)-(8) is indicative of the existence of an homoclinic orbit, but where the invariant object is a periodic solution rather than a fixed point. It is worth recalling that a homoclinic orbit of a system is given by the intersection of the stable W^s and unstable W^u manifolds of a saddle-type invariant

set [Kuznetsov *et al. (1998)*]. The stable manifold is defined as the set of all trajectories that tend to the invariant set in forward time and the unstable manifold is defined as the set of all trajectores that tend to the invariant set in backward time. A homoclinic orbit to a periodic solution is of codimension zero, such that the stable and unstable manifolds of the periodic solution intersect transversally and, consequently, the intersection persists under C^1 perturbations [Kuznetsov *et al. (1998)*]. A homoclinic orbit of a periodic solution can only be destroyed through a codimension-one homoclinic tangency. This occurs when the intersection of the stable and unstable manifolds becomes tangential and, thus, a small perturbation can separate the manifolds completely. A transition between a homoclinic orbit of a saddle-focus type steady-state and a homoclinic orbit of a periodic solution occurs at a codimension-two Šil'nikov-Hopf bifurcation [Hirschberg and Knobloch (1993)].

In two-parameter space this gives a transition from a one-dimensional locus (the codimension-one homoclinic orbit of a steady-state) to a two-dimensional area (the codimension-zero homoclinic orbit of a periodic solution); and this is what is observed in Fig (8). The inset of Fig(s) (7)-(8) show time series of several periodic solutions along the accumulating branch. These oscillations undergo an infinite sequence of saddle-node bifurcations, where these are represented at points Fig (7:a-d)-Fig (8:a-d) and the period of the periodic solutions increases without limit as it approximates the homoclinic orbit itself. In this case, the limit solution will be an unstable periodic orbit. The folds of the accumulating branches converge exponentially to a pair of codimension-one points, namely the homoclinic tangencies associated with the homoclinic orbit. Consequently, the accumulating branches of homoclinic orbit of a periodic solution remain of finite width in parameter space. In addition, a periodic solution of sufficiently large period at a fold of the accumulating branch can be used to approximate the respective homoclinic tangency. Selecting the point, Fig (8:d), as an approximate homoclinic tagency and by employing Newton's method (as implemented in DDE-Biftool) we find that the underlying periodic orbit converges to the point denoted UZ in the inset of Fig (9).

We replot this continuation diagram in Fig (9), emphasising the importance of the Hopf bifurcations HB_3 and HB_5 and the emanating branch of periodic solutions, which UZ is part of. Thus, the Hopf bifrucation, HB_3, is born from the lower unstable steady state and gives rise to a branch of unstable periodic orbits. Upon further increase in the parameter of interest, ν_{se}, the branch meets a saddle-node of periodic orbit (SNP_3). At this stage a decrease in the control parameter will see an increase in amplitude of the oscillations until UZ is encountered, as depicted in the left inset of Fig (9). Further decreasing ν_{se} results in an increase in amplitude as the branch passes through the stable region, $SNP_2 - PD_6$. However, note that the unstable periodic solutions emanting from HB_3 will not intersect the stable solutions that arise from the branch $SNP_2 - PD_6$, neither will these solutions meet at the saddle-node of periodic orbit SNP_2. Further continuing this branch of unstable periodic orbit by decreasing ν_{se} we observe that the branch vanishes at HB_5 where it switches back to unstable steady state as shown in the right inset of Fig (9). The same qualitative behaviour is observed for the Hopf bifurcations HB_2 and HB_4, however the resulting branches do not approach the accumulating branches.

We now return to our principal discussion about spike-wave oscillations and the role played by the delay in shaping these complexes. As we have described, the deformation from oscillatory behaviour to a full spike-wave morphology is due to a change in curvature arising via an inflection point, as the parameter ν_{se} is increased. In our previous study [Breakspear *et al. (2005)*] we argued that the delay arising from cortico-thalamic pathways was crucial in generating spike-wave oscillations. Hence, we complete this study by combining the inflection point criteria, bifurcation parameter ν_{se} and the delay into a single explanatory picture to characterise the appearance of spike-wave in the model. To this end, in DDE-Biftool we implement a well-posed periodic boundary value problem (pBVP) as defined in Appendix-(§A.4), by adding a functional that acts on the vector field (11). The pBVP (15) makes it possible to trace out branches in parameter space, corresponding to periodic solutions which satisfy the

inflection point criteria (obtained by simultaneous zero crossings of the numerically evaluated first and second derivatives). Specifically, we perform a two-parameter (ν_{se}, τ) continuation of such solutions and a hyperbolic-like curve emerges as shown in Fig (10). This curve, corresponds to the birth of the spike, with only the wave component visibly discernible when considering numerically generated time-series data from the model (As per the three insets of Fig (10). Moreover, the wave component remain invariant except when the hyperbolic curve crosses marked special points, resulting in a change in amplitude or frequency of the solution. These points occur when system eigenvalues change configuration, for example two eigenvalues within the unit disk merge (as is the case for the left point) or the system undergoes a period doubling (as for the second point). The top inset of Fig (10) shows that for large delays the frequency of the oscillations increases substantially and the region around the point from which the spike emanates becomes almost flat, with a corresponding shrinkage of the wave component. To compliment these results we compute numerically a bifurcation diagram, depicted in Fig (11), for uniformly increasing ν_{se} and a large delay $\tau = 0.25$. The geometry of the bifurcation resembles Fig (2), however the Hopf bifurcation, heralding the onset of abnormal activity, occurs for reduced values of the parameter ν_{se} and the small window of chaotic behaviour vanishes . In addition, there is a larger range of ν_{se} for which spike-wave activity is observed. The bottom left inset of Fig (11) illustrates such a time series, with a long plateau and narrow wave complex generated for $\nu_{se} = 0.003$. For these large values of the delay, the 'spike' arising as a result of the inflection point, does not readily relate to observed data, which is in keeping with the unphysiologically high values of the delay τ chosen. The bottom right inset of Fig (11) shows a time profile of the periodic solutions for $\nu_{se} = 0.0059$ and interestingly a small oscillation develops on the plateau of the overall wave form.

On the other hand, numerically computing bifurcation diagrams for a smaller delay (e.g. $\tau = 0.01$) shows that the Hopf bifurcation occurs for larger values of ν_{se} and the chaotic window also disappears (as depicted in Fig (12)). Furthermore, the parameter range within which spike-wave complexes are

observed, narrows and eventually vanishes for small enough delays. In this case, only periodic oscillations are observed. This provides further evidence of the importance of the delay in generating spike-wave activity in models of this type.

From a clinical perspective, the exact moment of initiation of an absence seizure remains poorly characterised. Generally the onset of the seizure is determined via analysis of scalp EEG and flagged up following the appearance of discernible spike-wave activity in the data. This characterisation of seizure onset has a number of shortcomings. Firstly, spike-wave oscillations may reflect an advanced state of the seizure when all neurons have entered a hypersynchronised state and the oscillations have propagated from the thalamus to the cortex. Secondly, the signal observed on the scalp is noisy, non-stationary, nonlinear and varies from patient to patient making an empirical onset characterisation inaccurate, as well as presenting significant challenges to automated seizure detection algorithms. From this perspective, the model predicts that the seizure onset is not associated with a change of the 3Hz EEG wave morphology. Instead, the findings we present suggest that the inflection point (corresponding to the onset of the spike) represents hypersynchronisation, namely an advanced state of the seizure, whilst the onset is determined by a Hopf bifurcation. Incorporating information from models of this type may provide an enhanced means for clinically characterising the onset of seizures.

5 Conclusions and future work

In this paper, we extend our previous work modelling human cortico-thalamic neuronal networks to investigate the onset of absence seizures [Breakspear *et al. (2005)*, Rodrigues *et al. (2006)*]. Making use of the numerical continuation packages DDE-BIFTOOL and PDDE-CONT allows us to complete the picture of the unfolding of spike-wave activity in these mean-field models. Most importantly, although we have previously shown that the periodic orbit arises from a Hopf bifurcation this is not the case for the spike component. We now find that the appearance of the spike does not result from a change in

structural stability as a parameter(s) is varied (bifurcation). Rather, an extra spike per period is born out of a smooth deformation of the oscillations via an inflection point, as the parameter of interest is varied. This is confirmed via evaluation of a well-posed boundary value problem that is setup in DDE-BIFTOOL allowing a curve in parameter space to be mapped out, corresponding to a family of solutions satisfying the inflection point criteria. Numerical simulations of the model confirm that spikes appear when crossing through this boundary.

This finding is borne out when studying some EEG traces from humans with absence epilepsy. The spike component of a 3Hz spike and wave complex can emerge as a smooth transformation from a signal that otherwise resembles a simple oscillation. Figure 13 illustrates a case in point. The 3Hz oscillation onsets with apparent discontinuity from the pre-ictal EEG. The spike, however, is not seen at first and subsequently emerges with smoothly increasing amplitude from the quasi-periodic waveform. To relate this to the behaviour of the model, we might say that the parameter ν_{se} varies smoothly between the bifurcation and the inflection point over the first $\sim$1s of the discharge. Figure 14 shows a different seizure. Here, the 3Hz activity changes abruptly in what appears to be a chaotic region, before briefly reemerging 5 seconds later and then returns to the 'resting' state (see the spectrogram). This is again what we might expect in the model if the parameter varied continuously during the course of the seizure ramping up to values past the period doubling bifurcations. Furthermore, some absence seizure data show little or no spikes at all and only a change in amplitude and frequency is observed in the brains electrical activity. The model provides an explanation for this type of seizure; namely the parameter, ν_{se}, passes through the Hopf bifurcation point, but does not increase past the inflection point boundary. In all of these cases, it is not possible to apply a physiological interpretation to the dynamics underlying the modulation of this parameter. Consequently we simply speculate what possible time-course could account for the observed data.

In particular, the results we present suggests that it is the Hopf bifurcation that heralds the onset

of absence seizures and furthermore provides a means of decoupling the initiation of the seizure and the onset of spike-wave activity. Further clinical research is desirable to better relate the neurological condition and the clinical observable. By explaining the mechanisms underlying different observations from clinically recorded seizure data, the model suggests strategies that could be adopted in clinical protocols. For example new detection algorithms could be based around bifurcation tracking in clinically recorded data, flagging a seizure as occurring as the system passes through a Hopf bifurcation [Sieber and Krauskopf (2008)]. It also suggests that different treatment strategies may be more appropriate for different sub-classes of the syndrome.

Typically, absence seizures are not confined to a specific frequency or amplitude, instead clinical data displays noisy modulation of $3Hz$ oscillations. Clinical studies have demonstrated slowing down or drift in frequency and cycle-to-cycle variation in absence seizures and these contribute markedly to nonlinear signal characteristics [Schiff *et al. (1995)*]. The cortico-thalamic model qualitatvely captures this behaviour by exhibiting period doubling as well as chaotic oscillations upon varying the parameter ν_{se}. In this regime, we observe various spike-wave wave morphologies, including periodic 'spike-wave-spike' complexes and chaotic spikes.

In the present work we do not consider noise, however to appropriately relate our work to clinical data, stochastic components should be incorporated. Noise is introduced by means of fluctuating inputs, which propagates to all dynamical variables of the system. However, this approach can limit the validity of results related to dynamical correlation between model variables. It is planned that future work will consider stochastic components arising from internal variables, such as synaptic stenghts, firing densities etc.

Additionally, the model displays bistability between normal state and maximal firing rate for some values of ν_{se}. However, it is unlikely this could occur in absence seizure subjects as this could correspond to neuronal death if the neurons involved fired maximally. Thus, we assume that in human cortico-thalamic

systems, the parameters remain within restricted boundaries. The bistability in the model arises mainly due to the interaction between the pyramidal cells and the thalamic specific cells, which form a positive feedback loop. Conversely, paroxysmal oscillations are born mainly through thalamic interactions, where this was demonstrated in our previous work [Rodrigues *et al. (2007)*]. An easy way to see this is by equating the right hand of the vector field (11) to zero, which has the following form:

$$\begin{cases} \phi_e(t) = \varsigma(V_e(t)), \\ V_e(t) = \nu_{ee}\varsigma(V_e(t)) + \nu_{ei}\varsigma(V_e(t)) + \nu_{es}\varsigma(V_s(t)), \\ V_s(t) = \nu_{sn}\phi_n + \nu_{se}\varsigma(V_e(t)) + \nu_{sr}\varsigma(V_r(t)), \\ V_r(t) = \nu_{re}\varsigma(V_e(t)) + \nu_{rs}\varsigma(v_s(t)). \end{cases} \tag{9}$$

The last three equations in (9) define an invariant set around which the equilibriums solutions lie. Specifically, equation for, $V_e(t)$, clearly evidences that the term $V_e(t) = (\nu_{ee} + \nu_{ei})\varsigma(V_e(t))$ can give rise to one, two or three fixed points, V_e^*, since $\varsigma(.)$ is a monotonic increasing function. Future work to improve this aspect of the model would be to incorporate inhibitory interneurons in the cortex, which would act as physiological mechanism to prevent the cortex from firing maximally. Further studies of the model should consider the incorporation other physiological mechanisms, such as the inclusion of T-type Ca^{2+} currents, GABAergic receptors and different firing rates for all neuronal populations involved, which may have the effect of further enhancing model predictions. For example, some clinical data show polyspikes and wave morphology, a feature which we do not observe in this present model, but which is captured in an enhanced model that incorporates connections corresponding to GABAergic receptors [Marten *et al. (2008)*].

Finally, a curious phenomena about the model was captured by the continuation diagrams (5) and (6), showing that after the onset of period doubling cascade the system regains stability in a very tiny region of parameter space. Within this region a branch of stable periodic orbits, demarked as SNP_2-PD_6, display solutions having 'spike-wave-spike' morphologies, with the second spike having a prominent

amplitude that almost resembles a wave activity. Upon further increase of the physiological parameter, ν_{se}, the system becomes unstable again and leads to chaotic dynamics that is organised by an unstable homoclinic to periodic orbit. The homoclinic is an emerging feature of the model but only organises the unstable states and with that contributing to the overall chaotic dynamics. To further contribute to the understanding of generalised seizure in humans it would be interesting to further develop the work initiated in [Breakspear *et al. (2005)*]. In particular, to performe a linear homotopy continuation from the set of absence seizure parameters to those corresponding to tonic-clonic seizures. For instance, the homotopy could be defined as follows:

$$h : \mathbb{R} \to \mathbb{R}^P, \quad h(\mu) = \mu\nu_1 + (1-\mu)\nu_2, \tag{10}$$

where $\nu_1 \in \mathbb{R}^{15}$ is the set of absence seizure parameters and $\nu_2 \in \mathbb{R}^{15}$ is the set of tonic-clonic seizure parameters. The new introduced parameter, μ, is a single continuation parameter that allows to find curves in parameter space and unfold bifurcations from seizure type to another. Obtaining such a result not only would unify absence seizures and tonic-clonic seizures in one unique framework, but would also support the hypothesis that seizures may be viewed as bifurcations between distinct types of nonlinear dynamics [Lopes da Silva *et al. (2003)*, Wendling *et al. (2002)*].

6 Acknowledgment

SR would like to thank Mathieu Desroches and Frank Marten for some very helpful discussions. SR, MR ad JRT acknowledge financial support from the Leverhulme Trust Theoretical Neuroscience Network and the EPSRC via grant EP/D068436/01.

A Appendix

A.1 Mean-field cortico-thalamic model

The global(spatially invariant) mean-field delayed cortico-thalamic model is expressed as follows:

$$\begin{cases} \frac{d}{dt}\phi_e(t) = y(t), \\ \frac{d}{dt}y(t) = \gamma_e^2\left[-\phi_e(t) + \varsigma(V_e(t))\right] - 2\gamma_e y(t), \\ \frac{d}{dt}V_e(t) = z(t), \\ \frac{d}{dt}z(t) = \alpha\beta\left[-V_e(t) + \nu_{ee}\phi_e(t) + \nu_{ei}\varsigma(V_e(t)) + \nu_{es}\varsigma(V_s(t-\tau))\right] - (\alpha+\beta)z(t), \\ \frac{d}{dt}V_s(t) = w(t), \\ \frac{d}{dt}w(t) = \alpha\beta\left[-V_s(t) + \nu_{sn}\phi_n + \nu_{se}\phi_e(t-\tau) + \nu_{sr}\varsigma(V_r(t))\right] - (\alpha+\beta)w(t), \\ \frac{d}{dt}V_r(t) = v(t), \\ \frac{d}{dt}v(t) = \alpha\beta\left[-V_r(t) + \nu_{re}\phi_e(t-\tau) + \nu_{rs}\varsigma(v_s(t))\right] - (\alpha+\beta)v(t). \end{cases} \tag{11}$$

The principal state variables are ϕ_e (mean excitatory cortical field), V_s (averaged membrane voltage of the thalamic specific neurons) and V_r (membrane voltage of thalamic relay neurons). External sensory inputs or noise is projected onto the specific relay neurons.

A.2 Initial conditions employed in the model

These initial conditions are defined through linear stability analysis [Robinson *et al. (2002)*], which allows to place the system (11) in some unstable region of attraction where seizure can occur. Denoting

the cortico-thalamic model (11) by equation (8), then the initial condition $\varphi(t)$ is

$$\varphi : [-\tau, 0] \to \mathbb{R}^8 : \begin{cases} \phi_e(0) =< random >, \\ y(0) = 0, \\ V_e(0) = \varsigma^{-1}(< random >), \\ z(0) = 0, \\ V_s(t) = VS(\varsigma^{-1}(< random >)), \\ w(0) = 0, \\ V_r(0) = \nu_{re}\varsigma(\varsigma^{-1}(11)) + \nu_{rs}\varsigma(\nu_{rs}\varsigma(\varsigma^{-1}(< random >))), \\ v(0) = 0 \end{cases} \tag{12}$$

Where $< random >$ is a random variable and the inverse sigmoidal is defined in the following way

$$\varsigma^{-1}(< random >) = \theta + \frac{\sigma\sqrt{3}}{\pi} log(\frac{Q^{max}}{y} - 1). \tag{13}$$

and the pseudo-code for the $Vs(.)$ function follows the Newton's iteration scheme difined as

---

```
function Vs(double a)[
  integer i;
  integer namx=10;
  double  root=0;
  for(i=0; i< namx; i++)[
    x=nu_re*varsigma(a) + nu_rs*varsigma(root);
    ff=-root+*nu_sn*phi_n + nu_se*varsigma(a) + nu_sr*varsigma(x);
    fp=-1+nu_sr*nu_rs*varsigma^{'}(x)*varsigma^{'}(root);
    root=root-ff/fp;
  ]
  return (root);
]
```

Note that we run our simulations a constant input signal. That is the variance of the noise that projects to the specific relay cells is zeros, $\phi_n = 1$. $\varsigma^{'}$ is the derivative of ς with respect to voltage, which is defined as follows

$$\varsigma^{'} = \frac{d\varsigma(V)}{dV} = \frac{\frac{Q^{max}\pi}{\sqrt{3}\sigma} e^{\frac{-\pi}{\sqrt{3}}(\frac{V-\theta}{\sigma})}}{[1 + e^{\frac{-\pi}{\sqrt{3}}(\frac{V-\theta}{\sigma})}]^2} \tag{14}$$

A.3 Parameters values employed in the model

The parameters values used to simulate absence seizures are given in the following table:

Quantity	Description	*Absence seizures*
γ_e	Average ratio between pulse velocity and axon range.	100 s^{-1}
θ	Threshold of membrane potential before a cell fires.	0.015 V
σ	Standard deviation (versus voltage) of an ensembles firing rate.	0.006 V
Q^{max}	Average maximum firing rate of a cell.	250 s^{-1}
α	Receptor inverse of decay time of potential produced at synapse.	50 s^{-1}
β	Receptor inverse rise time of potential produced at synapse.	200 s^{-1}
t_0	Corticothalamic return time (complete return loop).	$80ms$
ν_{ei}	Inhibitory corticocortical coupling strength.	-18e-4 Vs
ν_{ee}	Excitatory corticocortical coupling strength.	10e-4 Vs
ν_{es}	Specific thalamic nuclei to cortical coupling.	32e-4 Vs
ν_{se}	Cortical to specific thalamic nuclei connection strength.	0.0044 Vs
ν_{sr}	Thalamic reticular to specific thalamic nucleus coupling strength.	-8e-4 Vs
ν_{sn}	Nonspecific subthalamic input strength into specific neurons.	20e-4 Vs
ν_{re}	Excitatory cortical to thalamic reticular nucleus parameter.	$16e-4$ Vs
ν_{rs}	Specific to reticular thalamic nuclei coupling strength.	6e-4 Vs

Table 1: Parameter values for Absence seizures.

A.4 Periodic boundary value problem

Mathematically, the periodic boundary value problem with the inflection point condition is defined as follows

$$\begin{cases} \frac{dx}{dt} = TF(x(t), x(t-1), \nu), \\ x(0) = x(1), \\ \frac{\partial F(x)}{\partial x} = \frac{\partial^2 F(x)}{x^2} = 0. \end{cases} \tag{15}$$

Where ν is the set of parameters and $F(.)$ is the vector field (11), rescaled to the time scale of the delay τ, hence we have the term $x(t-1)$. The parameter T is the unknown period of oscillation to be determined in the boundary value problem. The periodicity condition is given by $x(0) = x(1)$, that is, periodic oscillations are rescaled [0, 1] mesh points. The third equation in (15) defines the inflection point conditions. The exact implementation in DDE-BIFTOOL of the periodic boundary condition can be provided upon the readers request.

References

[Andrezejak *et al. (2001)]* Andrezejak, R. G., Laehnertz, K., Mormann, F., Rieke, C., David, P., Elger, C. E. (2001). Indications of nonlinear deterministic and finite-dimensional structure in time series of brain electrical activity: dependence on recording region and brain state. *Physical Review E* 64.

[Arndt (1989)] Arndt, H. (1989). Numerical solution of retarded initial value problems: Local and global error and stepsize control. *Numerical Mathematics* 43:343–360.

[Baker *et al. (1995)]* Baker, C. T. H., Paul, C. A. H., Willie, D. R. (1995). A bibliography on the numerical solution of delay differential equations. Technical report 269, University of Manchester.

[Breakspear *et al. (2005)]* Breakspear, M., Roberts, J. A., Terry, J. R., Rodrigues, S., Mahant, N., Robinson, P. A. (2006). A unifying explanation of primary generalized seizures through nonlinear brain modeling and bifurcation analysis. *Cerebral Cortex* 16:1296–1313.

[Breakspear and Terry (2002a)] Breakspear, M., Terry, J. R. (2002a). Detection and description of non-linear interdependence in normal multichannel human eeg. *Clin. Neurophysiol.* 113:735–753.

[Breakspear and Terry (2002b)] Breakspear, M., Terry, J. R. (2002b). Nonlinear interdependence in neural systems: Motivation, theory and relevance. *International J. Neuroscience* 112:1263–1284.

[Coenen and Luijtelaar (1986)] Coenen, A. M. L., van Luijtelaar, E. L. J. M. (1986). Two types of electrocortical paroxysms in an inbred strain of rats. *Neurosci Lett.* 70:393–397.

[Crunelli and Lersche (2002)] Crunelli, V., Leresche, N. (2002). Childhood absence epilepsy: genes, channels, neurons and networks. *Nat. Rev. Neurosci.* 3:371–382.

[Donober *et al. (1998)]* Danober, L., Deransart, C., Depaulis, A., Vergnes, M., Marescaux, C. (1992). Pathophysiological mechanisms of genetic absence epilepsy in the rat. *Prog. Neurobiol.* 55:27–57.

[Destexhe and Sejnowski (2001)] Destexhe, A., Sejnowski, T. J. (2001). *Thalamocortical Assemblies. How ion channels, single neurons and large-scale networks organize sleep oscillations.* Oxford University Press.

[Engelborghs *et al. (2001)]* Engelborghs, K., Luzyanina, T., Samaey, G. (2001). DDE-BIFTOOL v.200 user manual: A Matlab package for bifurcation analysis of delay differential equations. Technical report tw-330, Department of Computer Science, K. U. Leuven, Leuven, Belgium.

[Freeman (1975)] Freeman, W. J. (1975). *Mass Action In The Nervous System. Examination of the Neurophysiological Basis of Adaptive Behavior through the EEG.* Academic Press New York.

[Friston *et al. (1994)]* Friston, K. J., Jezzard, P., Turner, R. (1994). Analysis of functional mri time-series. *Hum. Brain Mapp.* 1:153–171.

[Hairer *et al. (1993)]* Hairer, E., Norsett, S. P., Wanner, G. (1993). *Solving ordinary differential equations I, nonstiff problems* Springer series computational mathematics, 2nd rev. ed.

[Hairer and Wanner (1996)] Hairer, E., Wanner, G. (1996). *Solving ordinary differential equations II, stiff and differential algebraic problems* Springer series computational mathematics, 2nd rev. ed.

[Hirschberg and Knobloch (1993)] Hirschberg, P., Knobloch, E. (1993). Šil'nikov-hopf bifurcation. *Physica D* 62:202–16.

[Jirsa and Haken (1996)] Jirsa, V. K., Haken, H. (1996). Field theory of electromagnetic brain activity. *Phys. Rev. Lett* 77:960.

[Kim and Pimenov (1997)] Kim, A. V., Pimenov, V. G. (1997). Numerical methods for time-delay systems on the basis of i-smooth analysis. *Computational Mathematics* 1:193–196.

[Kuznetsov *et al. (1998)]* Kuznetsov, Y., Kuznetsov, L., Marsde, J. (1998). *Elements of Applied Bifurcation theory* Springer-Verlag, New York.

[Lopes da Silva *et al. (2003)]* da Silva F. H. L., Blanes, W., Kalitzin, S. N., Parra, J., Suffczynski, P., Velis, D. N. (2003). Epilepsies as dynamical diseases of brain systems: Basic models of the transition between normal and epileptic activity. *Epilepsia* 44:72–83.

[Lopes da Silva *et al. (1974)]* Lopes da Silva, F. H., Hoeks, A., Smits, H., Zetterberg, L. H. (1974). Model of brain rhythmic activity. the alpha-rhythm of the thalamus. *Kybernetik* 15:27–37.

[Lopes da Silva and Pijn (1999)] da Silva, F. H. L., Pijn, J. P. (1999). Epilepsy as a dynamic disease of brain systems. *Adv. Neurol.* 81:97–104.

[Marescaux *et al. (1992)]* Marescaux, C., Vergnes, M., Depaulis, A. (1992). Genetic absence epilepsy rat from strasbourg: a review. *J. Neural Transm.* 35:37–69.

[Marten *et al. (2008)]* Marten, F., Rodrigues, S., Benjamin, O., Richardson, M., Terry, J. R. (2008). Onset of poly-spike complexes in a mean-field model of human eeg and its application to absence epilepsy. Submitted to Proc. Roy. Soc. Vol. A.

[Mormann *et al. (2005)]* Morman, F., Kreuz, T., Rieke, C., Andrzejak, R., Kraskov, A., David, P., Elger, C., Lehnertz, K. (2005). On the predictability of epileptic seizures. *Clin. Neurophys.* 116:569–587.

[Nunez (1981)] Nunez, P. L. (1981). *Electric Fields of the Brain* Oxford University Press.

[Paul (1992)] Paul, C. A. H. (1992). Developing a delay differential equation solver. *Applied Numerical Mathematics* 9:403–414.

[Robinson *et al. (2002)]* Robinson, P. A., Rennie, C. J., Rowe, D. L. (2002). Dynamics of large-scale brain activity in normal arousal states and epileptic seizures. *Physical Review E* 65.

[Robinson *et al. (1997)]* Robinson, P. A., Rennie, C. J., Wright, J. J. (1997). Propagation and stability of waves of electrical activity in the cerebral cortex. *Physical Review E* 56:826.

[Robinson *et al. (2001)]* Robinson, P. A., Rennie, C. J., Wright, J. J., Bahramali, H., Gordon, E., Rowe, D. L. (2001). Prediction of electroencephalografic spectra from neurophysiology. *Physical Review E* 63.

[Rodrigues *et al. (2007)]* Rodrigues, S., Gonçalves, J., Terry, J. R. (2007). Existence and stability of limit cycle in a macroscopic neuronal population model. *Physica D* 233:39–65.

[Rodrigues *et al. (2006)]* Rodrigues, S., Terry, J. R., Breakspear, M. (2006) On the gensis of spike-wave activity in a mean-field model of human thalamic and cortico-thalamic dynamics. *Physics Letters A* 355:352–357.

[Schiff *et al. (1995)]* Schiff, N. D., Victor, J. D., Canel, A., Labar, D. R. (1995). Characteristic nonlinearities of the 3/s ictal electroencephalogram identified by nonlinear autoregressive analysis. *Biol. Ceybern* 72:519–526.

[Sieber and Krauskopf (2008)] Sieber, J., Krauskopf, B. (2008). Control-based bifurcation analysis for experiments. *Nonlinear Dynamics* 51(3):365–377.

[Stam *et al. (1999)]* Stam, C. J., Pijn, J. P. M., Suffczynski, P., da Silva, F. H. L. (1999) Dynamics of the alpha rhythm: evidence for non-linearity? *Clin. Neurophysiol.* 110:1801–1813.

[Stam and Pritchard (1999)] Stam, C. J., Pritchard, W. (1999). Dynamics underlying rhythmic and non-rhythmic variants of abnormal, waking delta activity. *Int. J. Psychophysiol* 34:5–20.

[Stam *et al. (1997)]* Stam, C. J., T, van Woerkom C. A. M., Keunen, R. W. M. (1997). Non-linear analysis of the electoencephalogram in creutzfeldt-jakob disease. *Biol. Cybern.* 77:247–256.

[Steriade *et al. (1998)]* Steriade M., Amzica, F., Neckelmann, D., Timofeev, I. (1998). Spike-wave complexes and fast components of cortically generated seizures. ii. extra- and intracellular patterns. *J. Neurophysiol.* 80:1456–79.

[Steriade and Contreras (1998)] Steriade, M., Contreras, D. (1998). Spike-wave complexes and fast components of cortically generated seizures. I. role of neocortex and thalamus. *J. Neurophysiol.* 80:1439–55.

[Suffczynski (2000)] Suffczynski, P. (2000). Neural dynamics underlying brain thalamic oscillations investigated with computational models Ph.D. diss., Institute of experimental physics, department of physics, Warsaw University.

[Suggczynski *et al. (2004)]* Suffczynski, P., Kalitzin, S., da Silva, F. H. L. (2004). Dynamics of non-convulsive epileptic phenomena modeled by a bistable neuronal network. *Neuroscience* 126:467–484.

[Szalai *et al. (2006)]* Szalai, R., Stépán, G., Hogan, S. J. (2006). Continuation of bifurcations in periodic delay-differential equations using characteristic matrices. *SIAM Journal on Scientific Computing* 4:1301–1317.

[van Luijtelaar *et al. (2003)]* van Luijtelaar, E. L. J. M., Coenen, A. M. L. (2003). Genetic animal models for absence epilepsy: a review of the wag/rij strain of rats. *Behav. Genet.* 33:635–655.

[Wang *et al. (1995)]* Wang, X. J., Golomb, D., Rinzel, J. (1995). Emergent spindle oscillations and intermittent bursts firing in a thalamic model: Specific neuronal parameters. *PNAS* 92.

[Wendling *et al. (2002)]* Wendling, F., Bartolomei, F., Bellanger, J. J., F. B., Chauvel, P. (2002) Epileptic fast activity can be explained by a model of impaired gabaergic dendritic inhibition. *Eur. J. Neurosci.* 15:1499–1508.

[Wilson and Cowan (1972)] Wilson, H. R., Cowan, J. D. (1972). Excitatory and inhibitory interactions in localized populations of model neurons. *Biophysical Journal* 12:1–24.

[Wright and Liley (1996)] Wright, J. J., Liley, D. J. (1996). Dynamics of the brain at global and microscopic scales: Neural networks and the eeg. *Behav. Brain Sci.* 19:285–320.

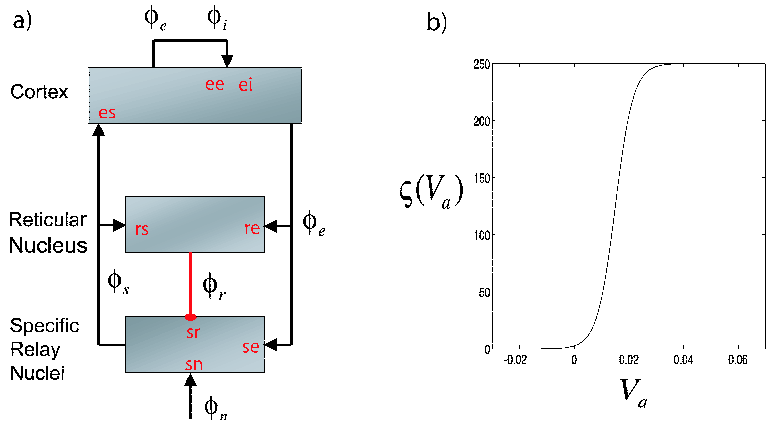

Figure 1: *a)Thalamocortical model, schema of principal neural fields and loops within the corticothalamic model. Fields include e=excitatory cortical; i=inhibitory cortical; s=specific thalamic nucleus; r=thalamic reticular nucleus; n=nonspecific subcortical noise. Connectivity and loops include intracortical (ee,ei), corticothalamic (er,se,es),intrathalamic (sr,rs) and ascending noise sn. b) The neurons (inhibitory and excitatory) are coupled by a unipolar sigmoidal function, which transforms the neurons transmembrane potential V_a (generally expressed as wave amplitude) into the firing rate $\varsigma(V_a)$ (termed pulse density), i.e voltage-frequency relation. Note the scale of the x-axes and y-axes (-0.03,0) to (0.07, 250). This is related to the averaging performed over a mm^3 of neural tissue, which is a highly nonlinear operation.*

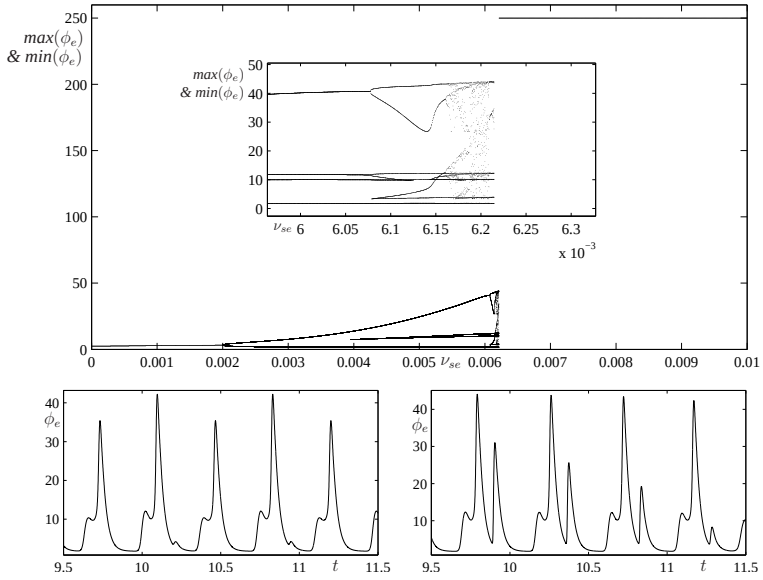

Figure 2: *The top panel illustrates numerical bifurcation diagram of the model (11) for absence seizure parameters as gathered in Table 1. Transition from healthy to seizure state is governed via a Hopf bifurcation. The model predicts chaotic regimes caused by period doubling cascades, which is detailed in the inset of top panel. The bottom panels illustrate numerical time series where the bottom left panel show oscillations at parameter* $\nu_{se} \approx 6.1 \times 10^{-3} Vs$ *whereas the right panel depicts chaotic oscillations for* $\nu_{se} \approx 6.2 \times 10^{-3} Vs$.

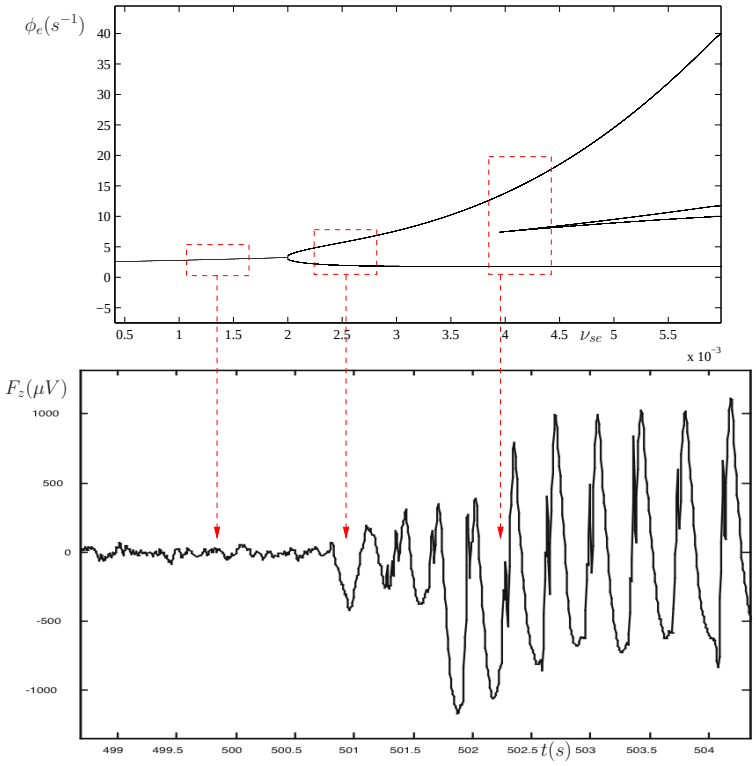

Figure 3: THIS FIGURE WILL BE UPDATED (Have to get data from Oscar)....Illustrating a comparison between bifurcation analysis of a mean-field model (Panel a) and a clinical EEG time trace at the onset of an absence seizure (Panel b). The model is noise-free and one sees as the bifurcation parameter ν_{se} is increased a transition from a steady state to an oscillatory regime via a Hopf bifurcation (around 0.002). Subsequently a further bifurcation (around 0.00375) to a spike-wave solution occurs. Contrast this with the clinical time-series where preictal the dynamics of the EEG are essentially a noisy steady state. Seizure onset commences with oscillatory behaviour (around 501 seconds), before exhibiting familiar spike-wave dynamics. The boxes indicate the regimes where the dynamics of the model correspond to those observed in the clinical time-series.

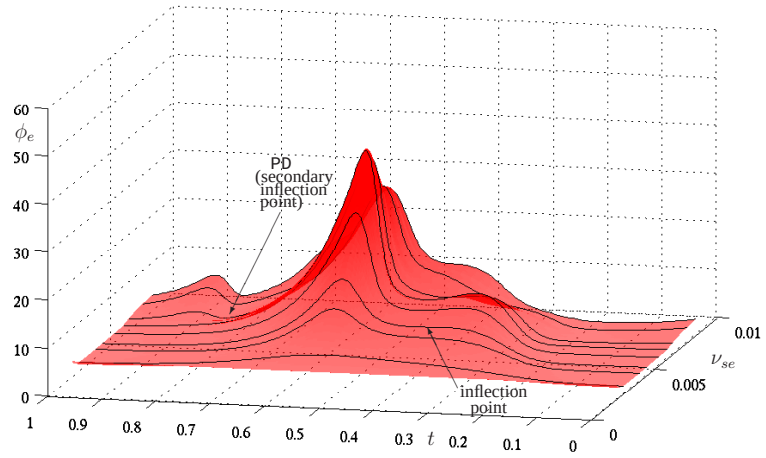

Figure 4: *The panel shows a one parameter family of pathologic oscillations. As the relevant physiological parameter ν_{se} is uniformly increased the oscillations deform smoothly from $3Hz$ sinusoidal paroxysmal oscillations to spike-wave rhythms via an inflection point. Upon further increase in ν_{se} a period doubling is born which give rise to a form of 'spike-wave-spike' complex.*

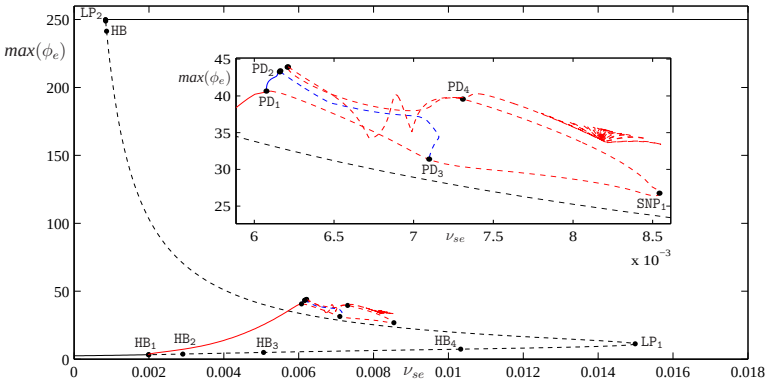

Figure 5: *An illustration of the global continuation diagram as computed by DDE-Biftool and PDDE-CONT. The maximal amplitude of the branches versus the physiological parameter ν_{se} is ploted and the solid lines represent stable branches whereas dashed represent unstable ones. The healthy steady state loses stability at the Hopf HB_1 but links to the upper maximal firing steady state through two fold points LP_1 and LP_2 where it regains stability. The branch of periodic solutions emanating from HB_1 increase in amplitude until it loses stability at a period doubling PD_1. The inset of the figure details how the branches are followed after PD_1, which depicts the branch folding back through a saddle-node of periodic orbit SNP_1 but then regains stability at a very narrow region in parameter space as explained in Fig (6). Further continuing the same branch it is observed that it folds back on itself numerous times until no further change is observed in the bifurcation diagram. Continuation of the period doubling is also explained via Fig (6).*

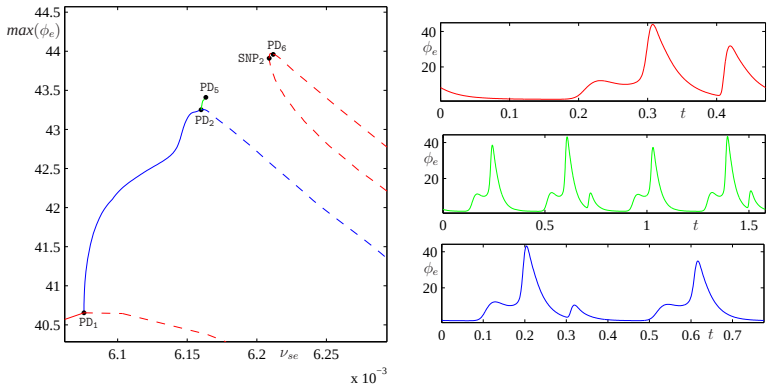

Figure 6: *The panel on the left is complementary to the continuation diagram shown in Fig (5). In this panel solid lines are stable peridic branches and dashed represent unstable orbits. A branch of periodic oscillations emanates from the period doubling PD_1, which increase in amplitude until a secondary period doubling PD_2 is encountered. An exemplar of the time series of the oscillations of this branch is shown in the right bottom panel, which show 'spike-wave-spike' followed by spike-wave complexes. The branch of periodic branch arising from PD_2 also sees an increase in amplitude until the period doubling PD_5 is found. An example of the time series of the this branch is depicted in the right middle panel which show the same wave oscillations as the previous branch however the period doubles. Following a sequence of period doubling becomes computationally very expensive thus the numerical simulations were halted. However the numerical bifurcation in Fig 2 supports that indeed we are in presence of period doubling cascade that leads to chaotic regimes. Comencing from PD_1 and following the unstable branch of periodic orbit (complimented by Fig (5)) it is observed that the branch regains stability through the saddle node of period orbit SNP_2 and yet loses stability at the period doubling PD_6. An illustration of the time series within the window SNP_2-PD_6 is shown in the right top panel, which indicates that the oscillations have 'spike-wave-spike' complexes with the second spike have a prominent amplitude.*

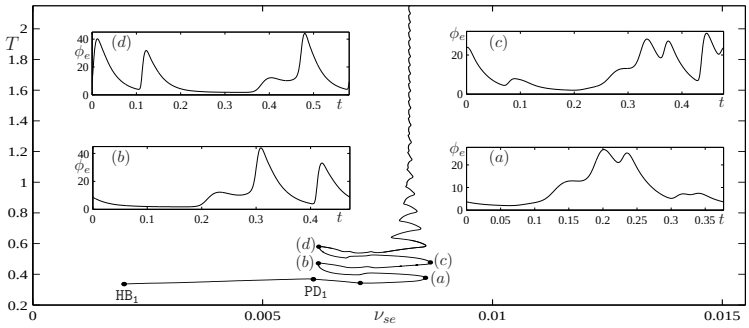

Figure 7: *An illustration of accumulating branches of periodic solutions close to a homoclinic orbit of periodic solution of saddle type. The branch is continued in (ν_{se}, T) parameter space where the period, T, tends to infinity. The branch initiates at the hopf bifurcation HB_1 and undergoes a period doubling PD_1 for increased values of ν_{se}. The branch undergoes infinite saddle-node bifurcations where representative markings are represented as a-d. The inset panels show time series of solutions along the saddle node.*

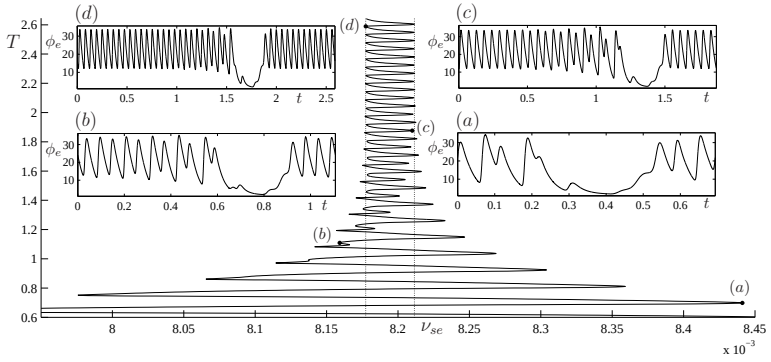

Figure 8: *This diagram is an enlargement of Fig 7 for higher values of the parameter T. The folds of the branch rapidly converge to one of two-parameter values (homoclinic tangencies) as shown by the vertical dotted lines. The inset panels show time series at the folds marked as a-d and for increasing values of T the solutions converge to the homoclinic orbit.*

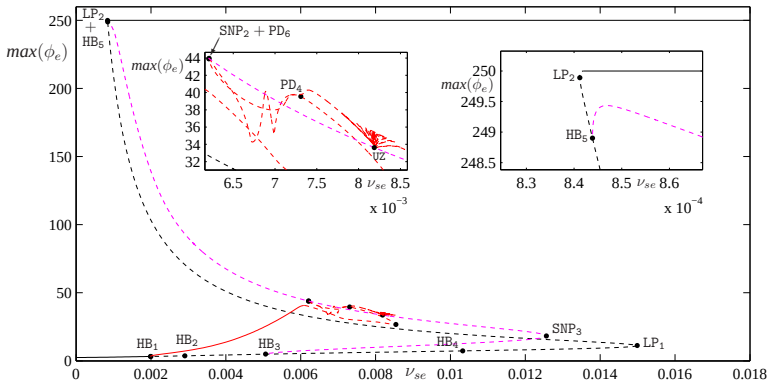

Figure 9: *This diagram is complementary to Fig 5, however focuses on the underlying periodic orbit of the homoclinic. Beyond the Hopf bifurcation HB_1 and upon further increase in parameter ν_{se} unstable Hopf bifurcations HB_2, HB_3 and HB_4 emerge. In particular HB_3 gives rise to a branch of unstable orbits that organise the behaviour of the homoclinic. As ν_{se} is increased the amplitude of the solutions augment until a saddle node of periodic orbit SNP_3 is encountered. Here the branch folds back but the branch does not regain stability. The left inset of the figure reveals more details when continuing along the branch for decreasing values of ν_{se}. The diagram shows that the unstable branch has a common solution, denoted UZ, to the homoclinic (seen as the red folding branch). This solution is the underlying unstable periodic orbit of the homoclinc. As ν_{se} is further decreased the branch continues through to the vicinity of the stable solutions SNP_2-PD_6 (compare with Fig (6), however without the solutions intersecting. The right inset of this figure details how the branches terminates at a Hopf bifurcation, HB_5, that merge with unstable stable branch.*

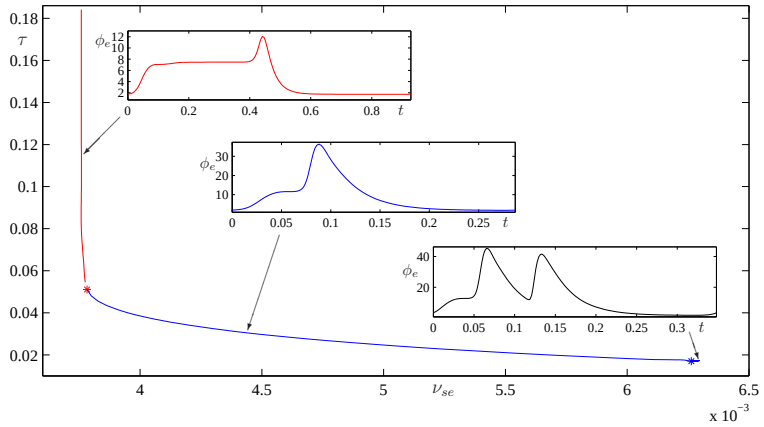

Figure 10: *A continuation branch in two parameter space, (ν_{se}, τ), of periodic solutions undergoing a curvature change in their solution profile due to inflection point. The continuation branch is a hyperbolic curve and all periodic solutions along the branch are about to initiate a spike. The marked asterisks represent a qualitative change in the solution profile due to the alteration in configuration of the eigenvalues of the model. However, note all solutions are stable. The three inset are representative time series for one period of oscillation as the delay and physiological parameter of interest are varied. For large delays and small physiological parameter the solutions, as shown in the top inset, tend to have a long plateu where a spike should be born. For decreasing delay the plateu shrinks and gives rise to the more characteristic wave form, however, without a spike yet. Upon further decrease in the delay and increase in the physiological parameter the model undergoes a period doubling and consequently a second bump in the solution is born. Under small perturbation of both parameters the solutions will have 'spike-wave-spike' complex.*

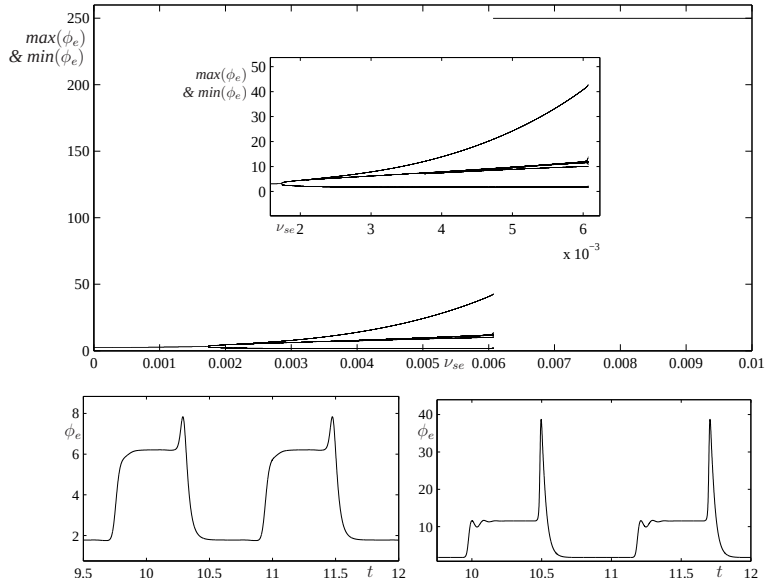

Figure 11: *The top panel illustrates numerical bifurcation diagram of the model (11) for increased delay value, i.e.* $\tau = 0.25$. *The diagram shows that the inflection point streches back until it meets the maximal amplitude of the paroxysmal oscillations as well as drifting the Hopf bifurcation to smaller values of* ν_{se} *and anhilating the chaotic regime. The bottom panels are examplers of the time series. When the inflection meets the maximal amplitude only sinusoidal like oscillations are observed. The bottom left panel is a time profile for* $\nu_{se} = 0.003$ *illustrating that the wave form has only long plateu where a spike should be born. The bottom right panel is time series for* $\nu_{se} = 0.0059$ *which interestingly shows a kind of oscillation developing in the plateau of the overall wave form.*

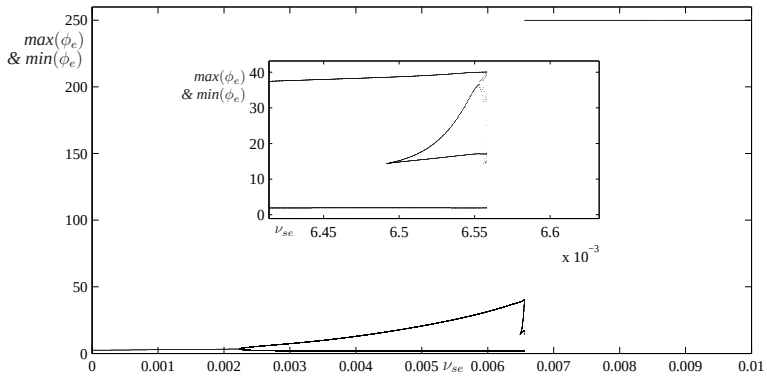

Figure 12: *The top diagram depicts a numerical bifurcation daigram for decreased delay value of* $\tau = 0.01$. *A decrease in delay causes the inflection point window to shrink and eventually vanishes for* $\tau = 0$ *where nnly sinusoidal like oscillations will be observed. The inset of the figure details the narrow region of inflection point and also the chaotic which exists for a narrow window of parameter values. The time series in this region are qualitatively equivalent to those oberved in Fig (2).*

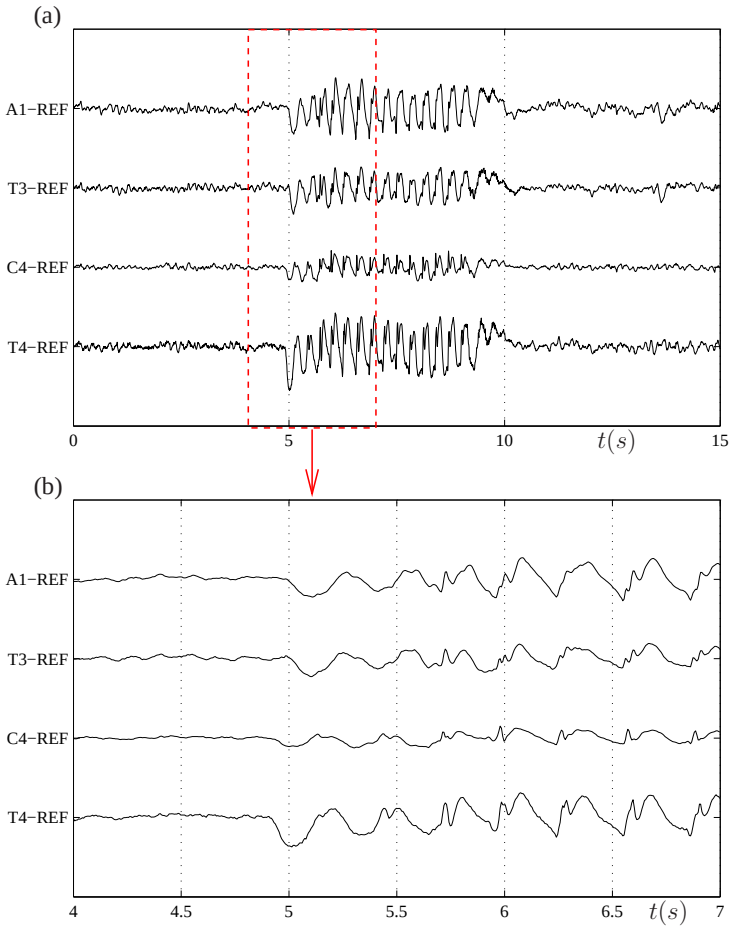

Figure 13: *Scalp EEG from human patient with childhood absence epilepsy. Panel a) 5 second ∼3Hz spike-wave discharge corresponding to a clinically confirmed absence seizure. At this scale the onset of the discharge (t=∼5s)appears abrupt compared with the previous EEG. Panel b): An enlargment of panel a. Closer inspection of the onset reveals that the onset of large amplitude* 3Hz activity *is abrupt. The* spike *component however is barely visible on the first cycle (see T4-REF at ∼5.2s) and increases smoothly in amplitude over the first few cycles. All channels shown are recorded with respect to a reference electrode located between Fz and Cz.*

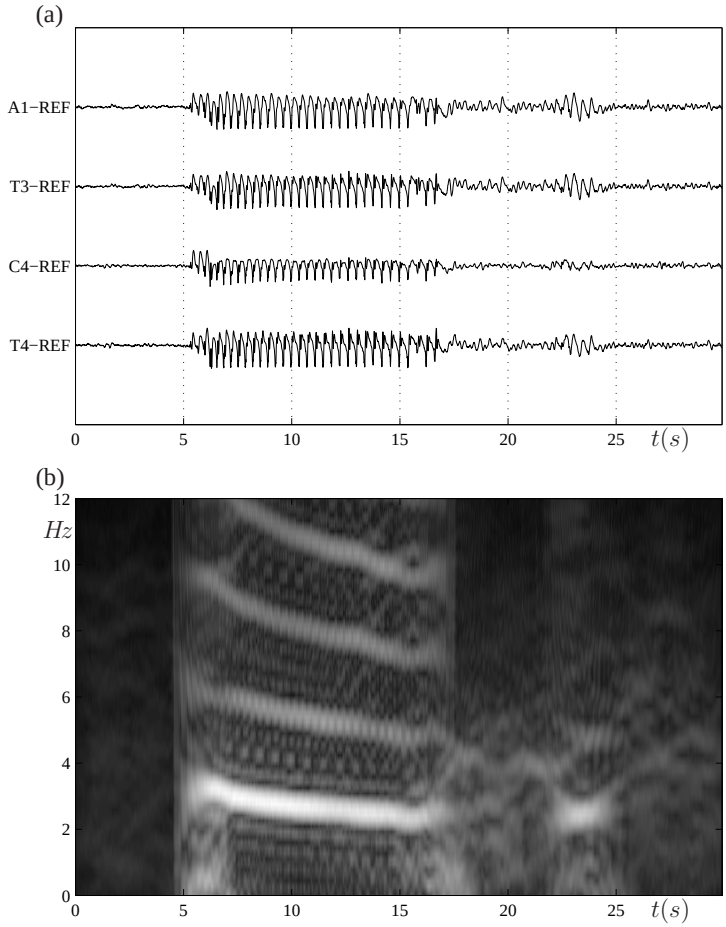

Figure 14: *Scalp EEG from human patient with childhood absence epilepsy (different patient from figure 13). Panel a) ∼3Hz spike-wave discharge corresponding to a clinically confirmed absence seizure. This discharge could be considered tobe 12s or 20s in duration as the definition of the offset is not obvious. The discharge EEG tranforms abruptly after 12s but similar activity briefly resurges 5s later. The latter activity has the same frequency but minimal spike-component and attenuates after 2-3s. Panel b) Average of spectrograms corresponding to all recorded EEG channels for the same discharge as A. Spectrograms computed from the discrete fourier transform of the signal after taking the inner-product with a Gaussian window with standard deviation 300ms. The time axis marks the centre of the of the window. Plot shows the average spectrogram computed from all 21 recording channels. The spectrogram makes clear that 3Hz activity terminates abruptly at 17s and re-emerges with the same frequency at 23-25s. The resurgent activity has minimal spike component and resembles a simpler oscillation as is apparent from the diminished signal power of the harmonic frequency components. All channels shown are recorded with respect to a reference electrode located between Fz and Cz.*